NEUROSCIENCE

Future spinal reflex is embedded in primary motor cortex output

Tatsuya Umeda[1,2,3]*, Osamu Yokoyama[4], Michiaki Suzuki[4], Miki Kaneshige[4], Tadashi Isa[1,5,6,7,8], Yukio Nishimura[1,4,8,9]*

Mammals can execute intended limb movements despite the fact that spinal reflexes involuntarily modulate muscle activity. To generate appropriate muscle activity, the cortical descending motor output must coordinate with spinal reflexes, yet the underlying neural mechanism remains unclear. We simultaneously recorded activities in motor-related cortical areas, afferent neurons, and forelimb muscles of monkeys performing reaching movements. Motor-related cortical areas, predominantly primary motor cortex (M1), encode subsequent afferent activities attributed to forelimb movement. M1 also encodes a subcomponent of muscle activity evoked by these afferent activities, corresponding to spinal reflexes. Furthermore, selective disruption of the afferent pathway specifically reduced this subcomponent of muscle activity, suggesting that M1 output drives muscle activity not only through direct descending pathways but also through the "transafferent" pathway composed of descending plus subsequent spinal reflex pathways. Thus, M1 provides optimal motor output based on an internal forward model that prospectively computes future spinal reflexes.

INTRODUCTION

Skillful hand and arm movements are attributed to sophisticated computations orchestrated within hierarchical neural networks (*1*, *2*). In the control of voluntary limb movements, motor cortex (MCx), consisting of premotor and primary motor (M1) cortices, acts as a higher-level motor controller responsible for generating muscle activity, while the spinal motor circuits act as a lower-level controller (*3*). Upper motor neurons in MCx project numerous axons to the spinal cord (*4*, *5*). The cortical descending output is transmitted to spinal motor neurons through direct cortico-motor neuronal connections and polysynaptic connections via spinal interneurons, ultimately culminating in the execution of limb movements. Despite extensive research correlating MCx activity with various motor-related physical parameters, the exact signals encoded by MCx remain elusive (*6*, *7*). Although recent advances in analyzing the neural dynamics of MCx successfully explain the transition from motor preparation to execution, the question of how the dynamic state of MCx population evolves to drive muscle activity remains unanswered (*8*–*11*). Consequently, the mechanism by which MCx controls limb muscle activity during voluntary limb movements remains an unsolved mystery (*7*).

In addition to MCx serving as a source of motor commands for spinal motor neurons, spinal reflex circuits also play a crucial role in generating muscle activity during voluntary limb movements (*12*–*15*). Various somatosensory receptors, including muscle spindles, tendon organs, joint receptors, and cutaneous mechanoreceptors, are passively activated by limb movements (*16*). These activations are subsequently transmitted to the spinal cord via peripheral afferents, which involuntarily modulate the activity of spinal motor neurons. Specific classes of spinal interneurons receive inputs from both MCx and somatosensory afferents and send outputs to spinal motor neurons (*17*). In addition, in macaque monkeys, a subset of spinal motor neurons directly receives projections from M1 and Ia afferents from muscle spindles (*18*–*20*). In other words, inputs from MCx and somatosensory afferents eventually converge on spinal motor neurons, which serve as the final common pathway. Thus, the motor hierarchy for activating limb muscles follows an intricate nested architecture rather than a strict serial structure.

During voluntary limb movements, the temporally and spatially organized convergence of inputs from MCx and peripheral afferents on spinal motor neurons underpins the generation of appropriate activity of limb muscles for the intended movement (*21*). Reflexive reactions to unexpected external changes are governed by the harmonious interplay between descending signals and spinal reflexes (*22*). These findings highlight the pivotal role of coordination between descending motor drive and somatosensory feedback signals in generating muscle activity. Several motor control theories, such as the servo control hypothesis (*23*), the internal model for motor control (*24*), and active inference (*25*), have been developed to encompass cortical voluntary control and reflexive modulation of limb muscles. Nonetheless, the neural mechanism by which MCx coordinates with spinal reflexes to control limb muscle activity under an intricate nested motor hierarchy remains to be elucidated.

Here, we explore the flow of neural information across MCx, peripheral afferents, and limb muscles during voluntary forelimb movements in monkeys to elucidate the neural mechanisms used by hierarchical motor controllers to regulate limb muscles. The information flow across the motor hierarchies indicates that MCx, in particular M1, encodes afferent activity and a subcomponent of muscle activity evoked by these afferent activities. Notably, selective interruption of peripheral afferents reduced this subcomponent. Our study reveals that M1 drives muscle activity by leveraging the

[1]Department of Developmental Physiology, National Institute for Physiological Sciences, National Institute of Natural Sciences, Okazaki, Aichi 4448585, Japan. [2]Department of Integrated Neuroanatomy and Neuroimaging, Graduate School of Medicine, Kyoto University, Kyoto 6068501, Japan. [3]Department of Neurophysiology, National Center of Neurology and Psychiatry, Kodaira, Tokyo 1878502, Japan. [4]Neural Prosthetics Project, Tokyo Metropolitan Institute of Medical Science, Setagaya, Tokyo 1568506, Japan. [5]Department of Neuroscience, Graduate School of Medicine, Kyoto University, Kyoto 6068501, Japan. [6]Human Brain Research Center, Graduate School of Medicine, Kyoto University, Kyoto 6068507, Japan. [7]Institute for the Advanced Study of Human Biology (WPI-ASHBi), Kyoto University, Kyoto 6068510, Japan. [8]School of Life Science, The Graduate University for Advanced Studies (SOKENDAI), Hayama, Kanagawa 2400193, Japan. [9]PRESTO, Japan Science and Technology Agency (JST), Kawaguchi, Saitama 3320012, Japan.
*Corresponding author. Email: umeda.tatsuya.4n@kyoto-u.ac.jp (T.U.); nishimura-yk@igakuken.or.jp (Y.N.)

spinal reflex in addition to direct modulation of spinal motor neurons. Thus, M1 sends motor output based on an internal forward model that prospectively computes the future spinal reflex, thereby ensuring precise control of limb movements. Our findings elucidate a principle neural process through which interconnected neural structures collaborate to produce the intended behavior.

RESULTS

Multiple regions were simultaneously recorded during limb movement

To explore a coordinated interplay between descending motor drive and somatosensory feedback signals in voluntary limb movements, we conducted the simultaneous recordings of electrocorticographic (ECoG) signals from MCx, including M1 and dorsal (PMd) and ventral (PMv) premotor cortices, the activity of a population of peripheral afferents at the lower cervical level [25 to 39 units from C7 and C8 dorsal root ganglia (DRGs) of monkey T, and 11 to 15 units from C6 and C7 DRGs of monkey C], electromyographic (EMG) signals from the forelimb muscles (12 and 10 muscles from monkeys T and C, respectively), and kinematic signals from the forelimb joints (wrist, elbow, and shoulder) in two monkeys, as the monkeys performed reaching and grasping movements (Fig. 1) (*21*, *26*). An example of simultaneous multiregional recording data (monkey T, three trials) is illustrated in Fig. 1B. Cortical high-gamma activity is widely accepted to reflect the activity of the neuronal population below the electrode; thus, we analyzed high-gamma activity (60 to 180 Hz) in MCx (*27*). The alignment of the multiregional signals to the timing of movement onset indicates the relative onset timing of these signals (Fig. 1B). The high-gamma activity in MCx and

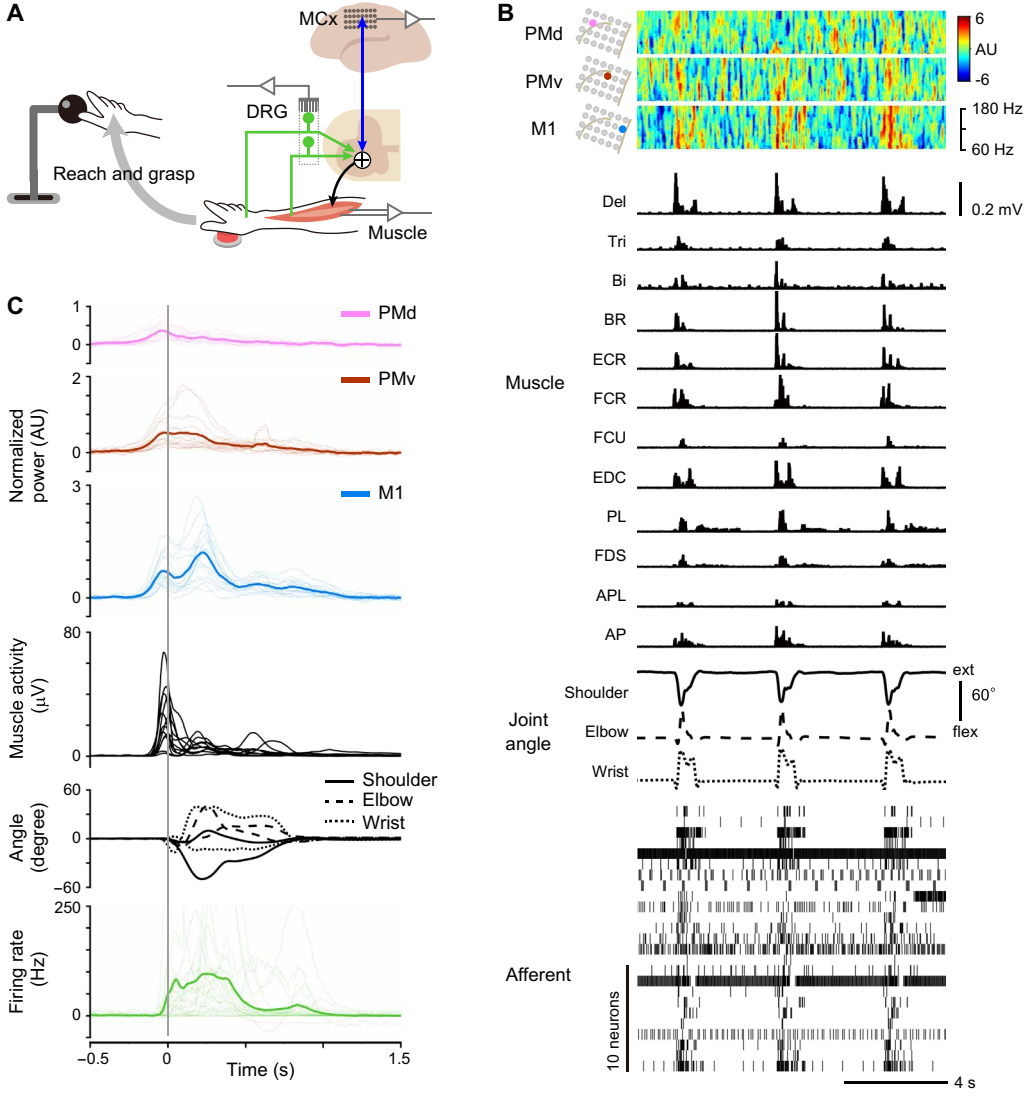

Fig. 1. Multiregional recordings during voluntary upper limb movements. (**A**) Experimental setup. (**B**) Simultaneous recordings in three trials. Top: Power spectrograms in MCx. Second: Activity of forelimb muscles. Third: Forelimb joint angles along the extension-flexion axis. Bottom: Raster plots of peripheral afferent activity. (**C**) Modulation of cortical and peripheral activity in monkey T aligned to movement onset. The average activity across 130 trials. Top to third: High-gamma cortical activity. Fourth: Forelimb muscles. Fifth: Joint angles. Bottom: Instantaneous firing rate of peripheral afferents. Thin lines represent the activity in each electrode (PMd, PMv, and M1), and units (afferent), and thick lines their respective averages. A vertical line represents the time of movement onset.

forelimb muscle activity increased before movement onset, and the neuronal firing of peripheral afferents started to undergo movement-related modulation at the time of movement onset (Fig. 1C).

MCx encodes reafferent signals

MCx sends descending control signals to spinal motor neurons to produce muscle activity for the execution of an intended movement (*6*). Muscle activation and subsequent joint movements further lead to the activation of peripheral afferents, which represents reafferent signals (*16*). According to this sequential flow of information, we reasoned that MCx activity is related to the generation of subsequent afferent activity evoked by limb movement (Fig. 2A). It has been well established that muscle activity can be explained by a linear sum of MCx activity that occurs 5 to 40 ms before the muscle activity to be calculated (*26*, *28*–*30*). Therefore, we assumed a delayed linear sum of MCx activity as a first-order model of afferent activity. By constructing a linear model to explain instantaneous afferent activity using MCx activity during the 40 ms preceding the timing of afferent activity, we were able to accurately reconstruct the overall temporal pattern of activity of a substantial number of peripheral afferents; this model outperformed models constructed using shuffled controls [correlation; monkey T (21 sessions), 51.9 ± 8.4 (mean ± SD) %; monkey C (7 sessions), 18.6 ± 6.1%, variance accounted for (VAF); monkey T, 48.2 ± 8.8%; and monkey C, 17.6 ± 6.1%; Fig. 2, B and C]. This result suggests that MCx activity encoded subsequent activity of peripheral afferents.

To determine the timing at which descending input was most strongly associated with subsequent afferent activity, we constructed models with different lead times from MCx activity to afferents activity and calculated the reconstruction accuracy of these models (Fig. 2, A and D). Calculating mean correlation coefficient and VAF using afferent data that could be reconstructed with high accuracy from MCx activity, MCx activity before approximately 75 ms (monkey T, 66.6 ms; and monkey C, 83.4 ms) was found to have an adequate lead time to explain subsequent afferent activity. These results suggest that MCx output is transmitted to peripheral afferents over 75 ms (red arrow in Fig. 2E).

Spinal reflex pathways convey MCx output

Our recent study revealed that afferent activity associated with forelimb movements contributed notably to muscle activity (green arrow in Fig. 2E) in conjunction with continuous MCx output during voluntary forelimb movements (blue arrow in Fig. 2E) (*21*). Among the recorded afferents, the afferent population, which were reconstructed by MCx activity (Fig. 2, B and C), contributed more to generation of muscle activity than other afferents (fig. S1). Considering that MCx output is transmitted to peripheral afferents (red arrow in Fig. 2E), we hypothesized that MCx output might modulate muscles in a delayed manner via the transafferent pathway, which is composed of the descending and spinal reflex pathways (yellow arrow in Fig. 2F), in addition to direct control via the descending pathway (blue arrow in Fig. 2F). Then, we sought to determine whether both the direct descending motor drive (descending input) and delayed action through the transafferent pathway from MCx (transafferent input) contribute to the generation of muscle activity. We posited a delayed linear sum of descending and transafferent inputs as a first-order model of muscle activity. A reasonable conduction time for most peripheral afferent activity in DRGs to reach spinal motor neurons is 5 to 40 ms (see Materials and Methods). By simply adding the

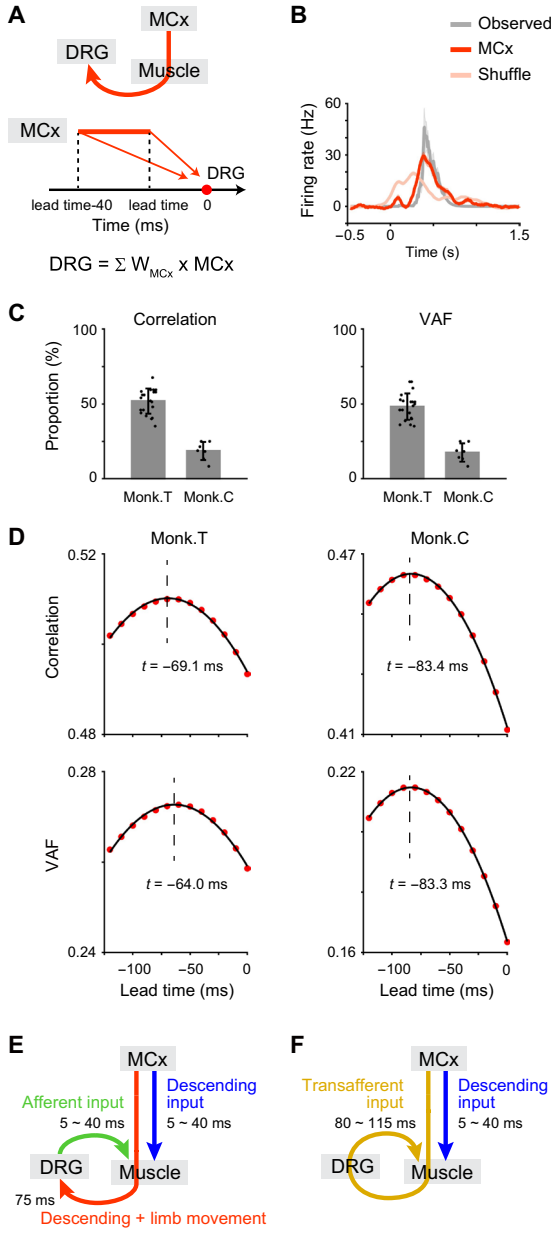

Fig. 2. MCx encodes reafferent signals. (**A**) Top: Model accounting for afferent activity in DRGs from MCx activity. Bottom: Temporal relationship between the descending input and afferent activity calculated from the input. (**B**) The observed activity of one example afferent, reconstruction using activity in MCx, and shuffled control data aligned to movement onset. The shaded areas indicate the SEM. (**C**) Proportion of afferents whose activities were more accurately reconstructed from MCx activity than from the shuffled data in the correlation coefficients and variances accounted for (VAFs) between the observed and reconstructed traces (monkey T, 21 sessions; and monkey C, 7 sessions). Data are the means ± SD. (**D**) Correlation coefficients and VAFs plotted against the lag times between afferent and MCx activity. The correlation coefficient or VAF of the model were averaged from the data of afferents for which the correlation coefficient or VAF of the model was superior to that of models built using a surrogate shuffled control and showed high accuracy (correlation coefficient greater than 0.4 and VAF greater than 0.15). The black line represents the fit to a quadratic curve. The vertical dotted lines indicate the lag time at the maximum value of the fitted curve. (**E**) Schematic illustrating a plausible sequence of information flow from MCx to muscles during voluntary movements. (**F**) Same as in (E), but MCx signals activate muscles via the descending pathway (blue) and via the transafferent pathway (yellow).

afferent conduction time (5 to 40 ms) to the time from MCx to afferents (75 ms) (Fig. 2E), we determined that most MCx activities require 80 to 115 ms to reach spinal motor neurons via the transafferent pathway (Fig. 2F). As mentioned, most MCx activity requires 5 to 40 ms to reach spinal motor neurons (*26*, *28*–*30*). Therefore, we constructed a linear model to explain the instantaneous muscle activity using the descending input for 5 to 40 ms and the transafferent input for 80 to 115 ms preceding the timing of muscle activity to be calculated (fig. S2A). The model accurately reconstructed the overall temporal pattern of muscle activity, outperforming models constructed using shuffled controls (fig. S2, B and C). Furthermore, the muscle activity calculated from both descending and transafferent inputs was reconstructed more accurately than that calculated from the descending input alone (fig. S2, D and E) or that calculated from descending and shuffled transafferent inputs (fig. S2, F and G). These results suggest that transafferent input is essential for the accurate reconstruction of muscle activity.

If MCx activity induces muscle activity via the transafferent pathway, which includes the spinal reflex pathway, the effects of delayed action through the transafferent pathway from MCx on muscles (yellow arrow in Fig. 3, A and B) must correspond to the effects of somatosensory feedback signals from peripheral afferents on muscles (green arrow in Fig. 3, D and E). To investigate this phenomenon, we decomposed the reconstructed muscle activity to identify the subcomponents of each input that affected the muscle activity. We calculated descending and transafferent components from the models built from the descending and transafferent inputs (Fig. 3C). To assess the effects of somatosensory feedback signals on muscles, we similarly constructed a linear model in which the descending input and activity of peripheral afferents (afferent input) together accounted for the subsequent muscle activity and yielded the descending and afferent components from the models (Fig. 3F). The temporal profile of the transafferent component was similar to that of the afferent component (Figs. 3, C and F, and 4, A and C). To evaluate the similarity, we used shuffled data of the transafferent input as controls for transafferent input and yielded the corresponding subcomponent (the shuffled components) (fig. S3, C and D). In addition, we used MCx activity at different time points relative to muscle activity to be analyzed (5 to 40 ms after the muscle activity) than the transafferent inputs as a control for the transafferent inputs, and derived the corresponding subcomponents (delayed components) (fig. S3, D and E). The similarity of the temporal profiles (temporal similarity) between the afferent and transafferent components was greater than the temporal similarity between the afferent and shuffled components and between the afferent and delayed components [monkey T (12 muscles), Desc + Transaff = 0.72 ± 0.03 (mean ± SEM), Desc + Shuffled = −0.03 ± 0.09, and Desc + Delayed = 0.23 ± 0.13; and monkey C (10 muscles), Desc + Transaff = 0.68 ± 0.05, Desc + Shuffled = 0.40 ± 0.10, and Desc + Delayed = 0.24 ± 0.07; Fig. 4E]. The temporal profile of the descending component in the model built from the descending and transafferent inputs was also similar to that of the descending component in the model built from the descending and afferent inputs [monkey T (12 muscles), Desc + Transaff = 0.99 ± 0.00, Desc + Shuffled = 0.97 ± 0.01, and Desc + Delayed = 0.90 ± 0.04; and monkey C (10 muscles), Desc + Transaff = 0.91 ± 0.08, Desc + Shuffled = 0.97 ± 0.02, and Desc + Delayed = 0.95 ± 0.02; Fig. 4, A, C, and E).

The size of the subcomponents varied across different muscles. We calculated the area above or below the baseline for each subcomponent during the period in which movement-related modulation of muscles was detected as the size of the subcomponents. The distribution of the transafferent component sizes across different muscles was

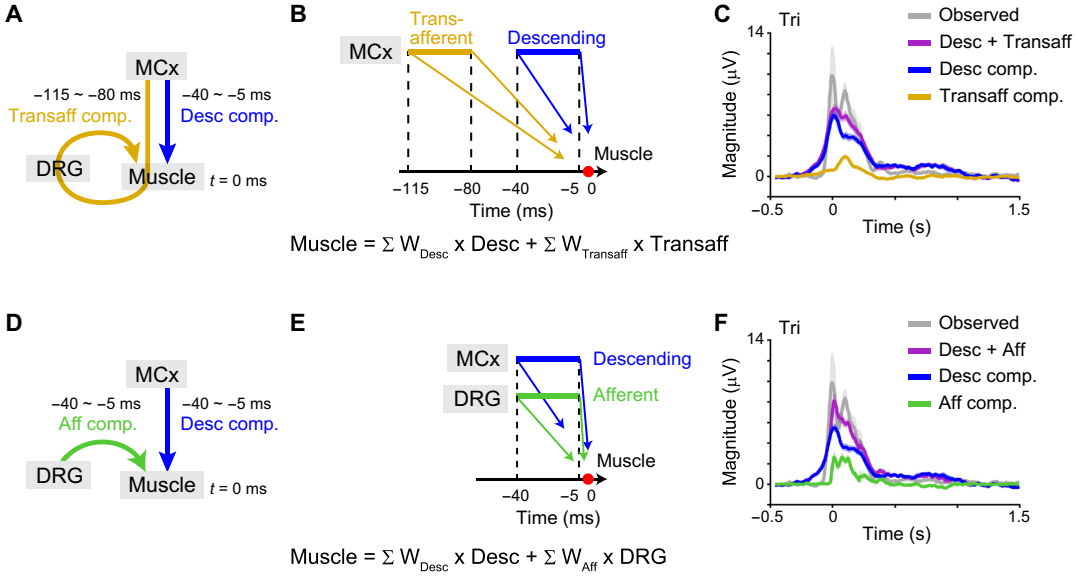

Fig. 3. Multivariate information decomposition elucidates subcomponents. (**A**) Models accounting for muscle activity evoked by descending and transafferent inputs. (**B**) Temporal relationship between the descending and transafferent inputs and muscle activity calculated from these inputs. (**C**) The observed muscle activity (triceps), its reconstruction using descending and transafferent inputs, and each subcomponent aligned to movement onset. Correlation coefficient between the observed muscle activity and the reconstruction using descending and transafferent inputs was 0.95. The shaded areas indicate the SEM. (**D** to **F**) Same as in (A) to (C) but for descending and afferent inputs, respectively. Correlation coefficient between the observed muscle activity and the reconstruction using descending and afferent inputs was 0.96.

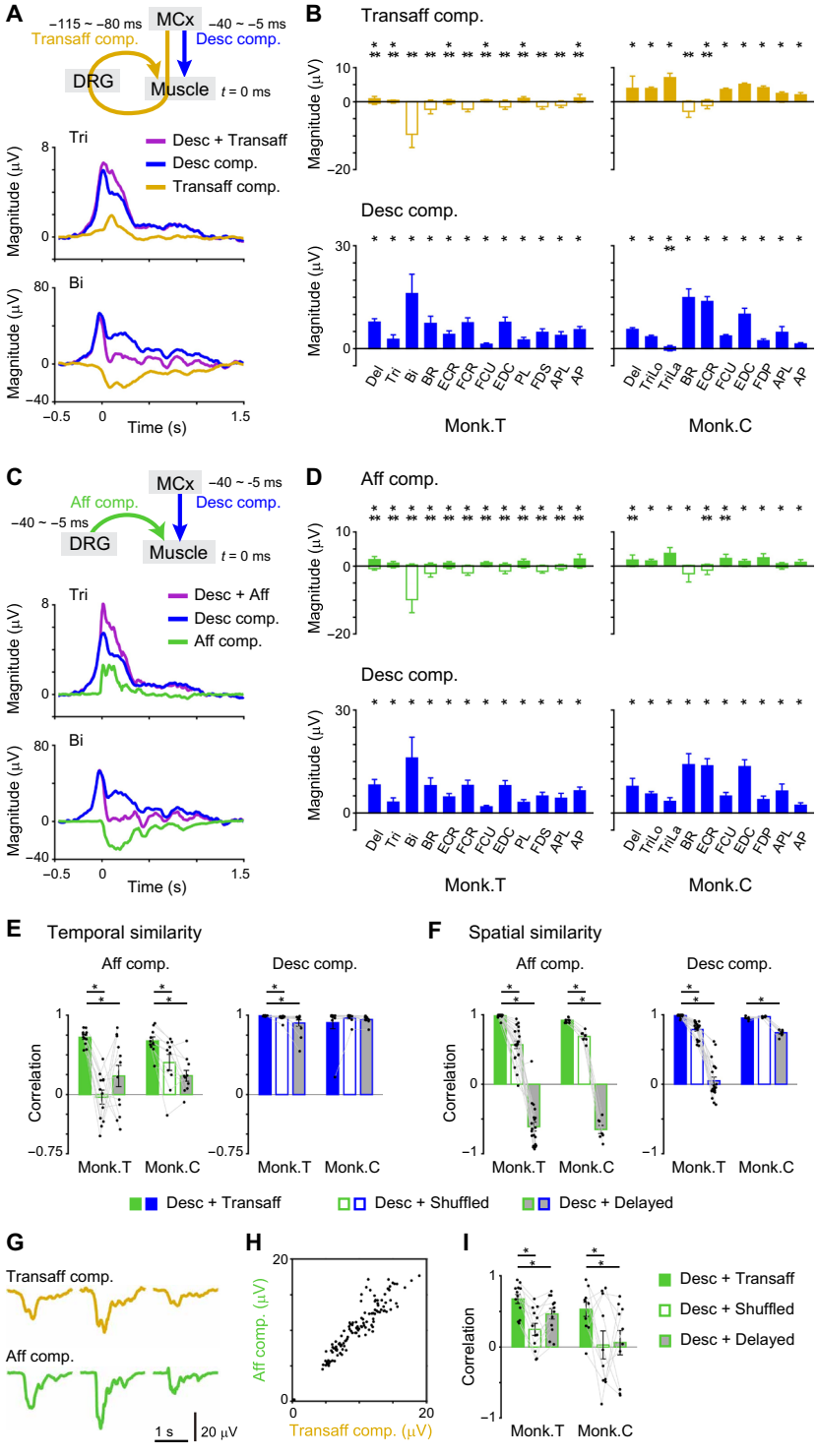

Fig. 4. MCx encodes the activation of muscles through the spinal reflex pathway. (**A**) Reconstruction using descending and transafferent inputs and each subcomponent aligned to movement onset. (**B**) Size of subcomponents (monkey T, 21 sessions; monkey C, 7 sessions). (**C** and **D**) Same as in (A) and (B) but for the descending and afferent components, respectively. (**E**) Temporal similarity between afferent and transafferent components (left) or across descending components (right) for different models (monkey T, 12 muscles; and monkey C, 10 muscles). (**F**) Same as in (E) but for the spatial similarity of afferent (left) or descending (right) components across muscles for different models (monkey T, 21 sessions; and monkey C, 7 sessions). (**G**) Transafferent and afferent components in three datasets. (**H**) Scatter plots of the size of transafferent versus afferent components. Dot, a single dataset. (**I**) Average correlation between afferent and transafferent components in the scatter plot for the different models (monkey T, 12 muscles; and monkey C, 10 muscles). In (B) and (D), data are the means ± SD. * and **$P < 0.05$, unpaired two-tailed t test for positive and negative values, respectively. In (E), (F), and (I), data are the means ± SEM. $P < 0.05$, one-way repeated-measures analysis of variance (ANOVA); *$P < 0.05$, paired two-tailed t test. P values are described in tables S1 to S5.

similar to that of the afferent component sizes (Fig. 4, B and D). The similarity of the distribution of afferent and transafferent components across muscles (spatial similarity) was greater than the spatial similarity between the afferent and shuffled components and between the afferent and delayed components [monkey T (12 muscles), Desc + Transaff = 0.98 ± 0.01, Desc + Shuffled = 0.57 ± 0.07, and Desc + Delayed = −0.61 ± 0.09; and monkey C (10 muscles), Desc + Transaff = 0.92 ± 0.01, Desc + Shuffled = 0.69 ± 0.02, and Desc + Delayed = −0.65 ± 0.05; Fig. 4F]. The spatial profile of the descending component in the model built from the descending and transafferent inputs was also similar to that of the descending component in the model built from the descending and afferent inputs [monkey T (12 muscles), Desc + Transaff = 0.98 ± 0.01, Desc + Shuffled = 0.79 ± 0.03, and Desc + Delayed = 0.05 ± 0.07; and monkey C (10 muscles), Desc + Transaff = 0.95 ± 0.01, Desc + Shuffled = 0.97 ± 0.00, and Desc + Delayed = 0.74 ± 0.02; Fig. 4, B, D, and F]. These results suggest that MCx activity between −80 and −115 ms before muscle activity encoded similar spatiotemporal information about muscle activity as does subsequent afferent activity.

The size of the afferent component was variable across datasets (Fig. 4G). If the effects of transafferent input on muscles correspond to afferent input, the variation in the size of the transafferent component across datasets should reflect the variation in the size of the afferent component. We found a positive correlation between the sizes of the afferent and transafferent components (Fig. 4H). The correlation between the size variation of the afferent and transafferent components was notably greater than those between the afferent and shuffled components and between the afferent and delayed components [monkey T (12 muscles), Desc + Transaff = 0.67 ± 0.06, Desc + Shuffled = 0.25 ± 0.09, and Desc + Delayed = 0.47 ± 0.07; and monkey C (10 muscles), Desc + Transaff = 0.53 ± 0.10, Desc + Shuffled = 0.03 ± 0.20, and Desc + Delayed = 0.06 ± 0.17; Fig. 4I]. Together, these findings suggest that MCx activity from −115 to −80 ms and from −40 to −5 ms before muscle activity encodes the muscle activity evoked by the afferent and descending inputs, respectively.

MCx encodes the stretch reflex and reciprocal inhibition

Next, we wondered whether the activation of limb muscles through the transafferent pathway corresponds to the action of spinal reflexes on limb muscles, such as the stretch reflex and reciprocal inhibition. Our previous study analyzing the relationship between initial limb movement and subsequent afferent components indicated that afferent effects on muscle activity conform to the pattern of spinal reflexes (*21*). For instance, monkey C initiated reaching by supination of the elbow joint and flexion of the wrist joint (Fig. 5A). The afferent component at the beginning of the reaching movement (55 to 100 ms around movement onset) exhibited a facilitatory effect on the elbow extensor, the triceps brachii lateralis (TriLa), and a suppressive effect on the elbow flexor, the brachioradialis (BR), which act as antagonists of the TriLa (Fig. 5, B and C). These antagonistic activations on the extensor and flexor muscles could be attributed to the stretch reflex and reciprocal inhibition, respectively. The results obtained from monkey T also indicated a similar relationship between initial joint movements and corresponding afferent components [monkey T (21 sessions), Tri = 3.53 ± 1.60 (mean ± SD) μV, Bi = −24.49 ± 11.34 μV, BR = −1.42 ± 3.73 μV, ECR = 3.77 ± 2.72 μV, and FCR = −7.65 ± 2.55 μV; and monkey C (7 sessions), TriLa = 8.62 ± 3.30 μV and BR = −4.45 ± 4.75 μV; Fig. 5C]. We subsequently investigated whether the transafferent effects on muscle activity could also be attributed to the stretch reflex and reciprocal inhibition. We calculated the transafferent component at the beginning of the reaching movement. Similar to afferent components, transafferent input exerted a facilitatory effect on some agonist muscles (elbow extensors) and a suppressive effect on antagonist muscles (elbow and wrist flexors in monkey T and an elbow flexor in monkey C) [monkey T (21 sessions), Tri = 1.74 ± 0.73 μV, Bi = −18.45 ± 8.74 μV, BR = −2.59 ± 2.98 μV, ECR = 1.24 ± 1.23 μV, and FCR = −4.70 ± 1.85 μV; and monkey C (7 sessions), TriLa = 13.84 ± 2.45 μV and BR = −5.91 ± 3.43 μV; Fig. 5C]. We calculated the shuffled or delayed components during the same period, but the results were not consistent with spinal reflex action (fig. S4). Therefore, the effects of transafferent inputs on muscle activity are at least partially accounted for by the action of spinal reflexes. These results further suggested that MCx encodes the spinal reflex.

M1 encodes the transafferent effect more than PMd or PMv

The corticospinal projections of primates play an important role in relaying motor commands from multiple motor-related areas to the spinal cord (*4*). Next, we asked which cortical area contributes to the generation of muscle activity through the transafferent pathway. By recording ECoG signals in PMd, PMv, and M1 with a multichannel electrode array, we were able to compare the effective activity across these areas. We calculated the descending and transafferent components based on the activity in each cortical area and found that the subcomponents calculated from M1 activity were much more prominent than the subcomponents calculated from PMd or PMv activity (Fig. 6, A to C, and fig. S5A). Similarly, the subcomponents calculated from M1 activity for the reconstruction of afferent activity were also more prominent than the subcomponents calculated from PMd or PMv activity (Fig. 6, A to C, and fig. S5A). M1 sites with the largest subcomponent for the transafferent input, which corresponds to the action of spinal reflexes, were located just anterior to the central sulcus, as was the case for the descending input and the afferent reconstruction (Fig. 6D and fig. S5B). Thus, the transafferent input from a subset of M1 rather than PMd or PMv could primarily account for muscle activity.

Transafferent M1 output drives muscles

If M1 signals transmitted by the transafferent pathway are crucial for driving muscle activity, selective blockade of the transafferent pathway should result in a reduction in muscle activity, especially its transafferent component. We tested this possibility by sectioning peripheral afferents (i.e., performing dorsal rhizotomy) at the lower cervical level (C6-C8), which innervate the forearm, in two other monkeys (Fig. 7A). Dorsal rhizotomy causes large-scale reorganization of neural circuits through axonal sprouting, which takes several weeks (*31*, *32*). To minimize such long-term effects on neural reorganization, we analyzed the data obtained immediately after dorsal rhizotomy (up to 5 days after dorsal rhizotomy). The attenuation of somatosensory evoked potentials (SEPs) elicited by electrical stimulation of forelimb muscles indicated blockade of most signal transmission from peripheral afferents (Fig. 7B). Following rhizotomy, the monkeys showed a diminished capacity for dexterous finger movements. However, they retained their ability to reach to the object with their affected limb and achieved a consistent success rate in their tasks. In addition, they were still capable of conducting the task within a similar overall timeframe, albeit with a temporary increase in their movement or reach time compared to prior performance

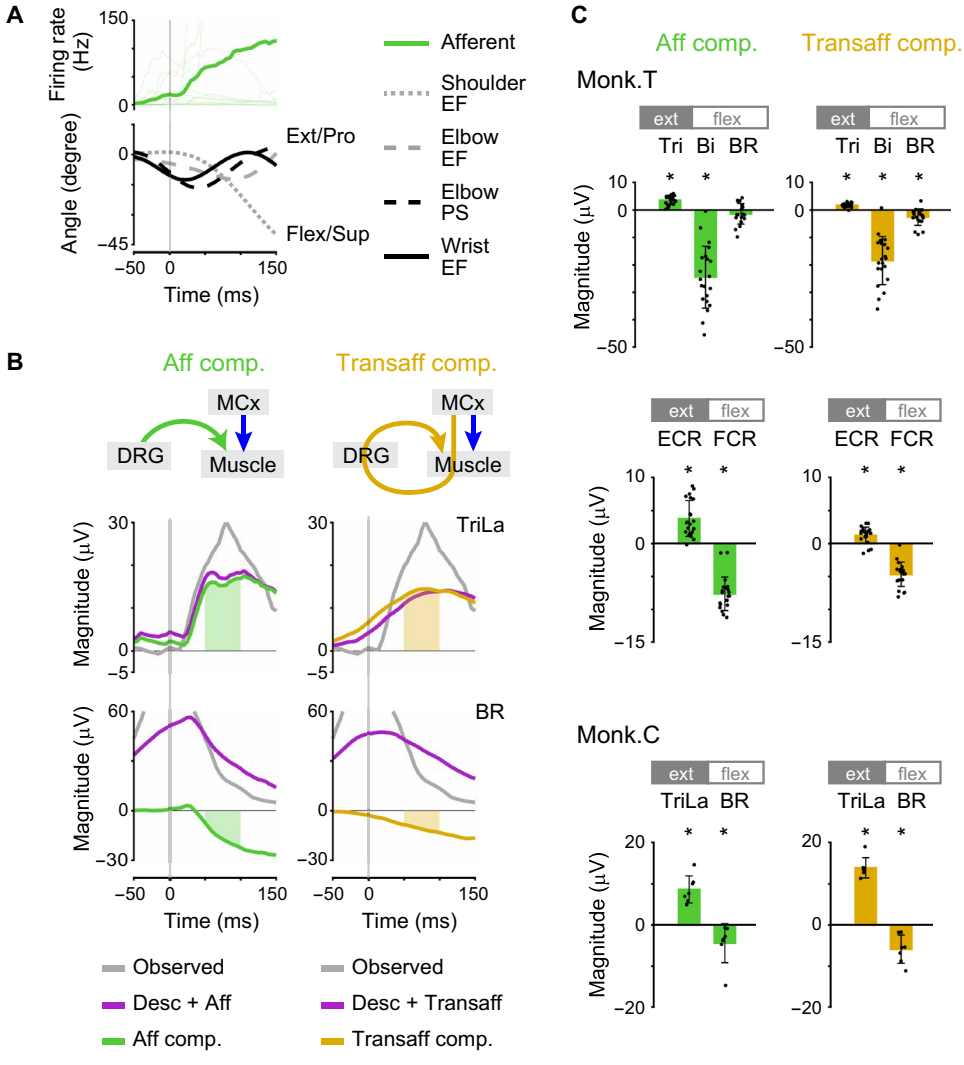

Fig. 5. The effects of transafferent input on muscles are accounted for by the stretch reflex and reciprocal inhibition. (**A**) Afferent activity and forelimb joint angles of monkey C when the monkey began to reach. EF, extension/ flexion; PS, pronation/supination. (**B**) Left: The observed muscle activity of monkey C, its reconstruction using descending and afferent inputs, and the afferent component of the reconstruction. The vertical lines indicate the time of movement onset. Right: The observed muscle activity, its reconstruction using descending and transafferent inputs, and transafferent component in the reconstruction. (**C**) Size of afferent (left column) and transafferent (right column) components for antagonistic muscle pairs (ext, extensor; and flex, flexor) in a period from the beginning of the reaching movement [55 to 100 ms around movement onset; shown in the green and yellow areas in (B), monkey T, 21 sessions; monkey C, 7 sessions]. Data are the means ± SD. *$P < 0.05$, unpaired two-tailed *t* test. *P* values are described in table S6.

[monkey P (movement time), intact (3820 trials) = 0.80 ± 0.86 (mean ± SD) s and rhizotomy (1500 trials) = 0.91 ± 0.23 s; and monkey B (reach time), intact (2100 trials) = 0.24 ± 1.1 s and rhizotomy (1400 trials) = 0.26 ± 0.46 s; fig. S6A).

We recorded activity in MCx and the forelimb muscles when the monkeys performed reaching movements before and after dorsal rhizotomy (fig. S6B). The total muscle activity and the peak amplitude of muscle activity during movements decreased after dorsal rhizotomy [monkey P (13 muscles), intact = 124.1 ± 16.5 (mean ± SEM) mV and rhizotomy = 105.5 ± 14.7; and monkey B (12 muscles), intact = 116.3 ± 16.0 and rhizotomy = 60.3 ± 8.9; gray lines in Fig. 7, C to E, and fig. S7A]. These findings suggested that afferent inputs transmitted through the somatic reflex arc contribute to the activation of forelimb muscles during voluntary movements.

Next, to examine whether dorsal rhizotomy affects the transafferent descending activation of muscles, we constructed a linear model using descending and transafferent inputs to account for the subsequent muscle activity and calculated the descending and transafferent components. The model reconstructed the overall temporal pattern of muscle activity before and after dorsal rhizotomy with a similar degree of accuracy (fig. S7B), and also reconstructed it more accurately than the shuffled control (fig. S7, C and D). Among the motor-related areas, M1 encodes the most information on muscle activity transmitted via the direct descending and transafferent pathways in monkeys P and B (fig. S8). We calculated the size of the transafferent component during movement and found that it decreased after dorsal rhizotomy [monkey P (13 muscles), intact = 56.5 ± 9.1 and rhizotomy = 36.2 ± 5.3; and monkey B

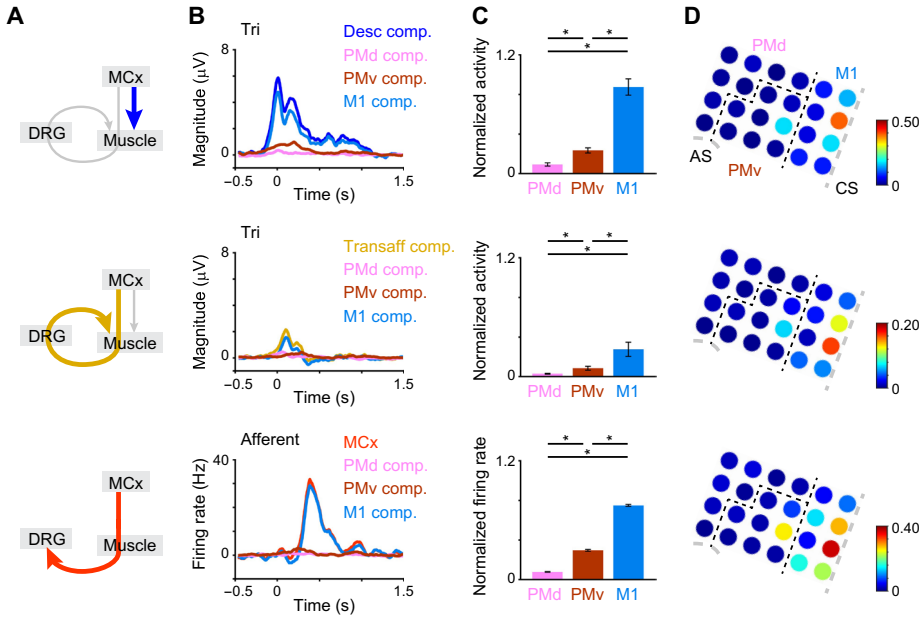

Fig. 6. M1 is a major predictor of muscle activity by descending and transafferent pathways. (**A**) The thick, colored arrows show the inputs for which the modulation is represented in (B) to (D). (**B**) Top and second: Reconstruction of muscle activity using descending and transafferent inputs and subcomponents calculated from the activity in each cortical area aligned to the movement onset of monkey T. Bottom: Reconstruction of afferent activity using MCx activity and subcomponents calculated from the activity in each cortical area aligned to the movement onset of monkey T. (**C**) Size of subcomponents calculated from the activity in each cortical area for the prediction of muscle or afferent activity (monkey T, 12 muscles or 702 afferents). (**D**) Color maps representing the size of subcomponents calculated from the activity at each electrode for the prediction of muscle or afferent activity in monkey T. The size of each subcomponent is normalized by the extent of the reconstruction of muscle activity using the descending and transafferent inputs or the reconstruction of afferent activity using the descending input. CS, central sulcus; AS, arcuate sulcus. In (C), data are the means ± SEM. $P < 0.05$, one-way repeated-measures ANOVA, $^*P < 0.05$, paired two-tailed t test. P values are described in table S7.

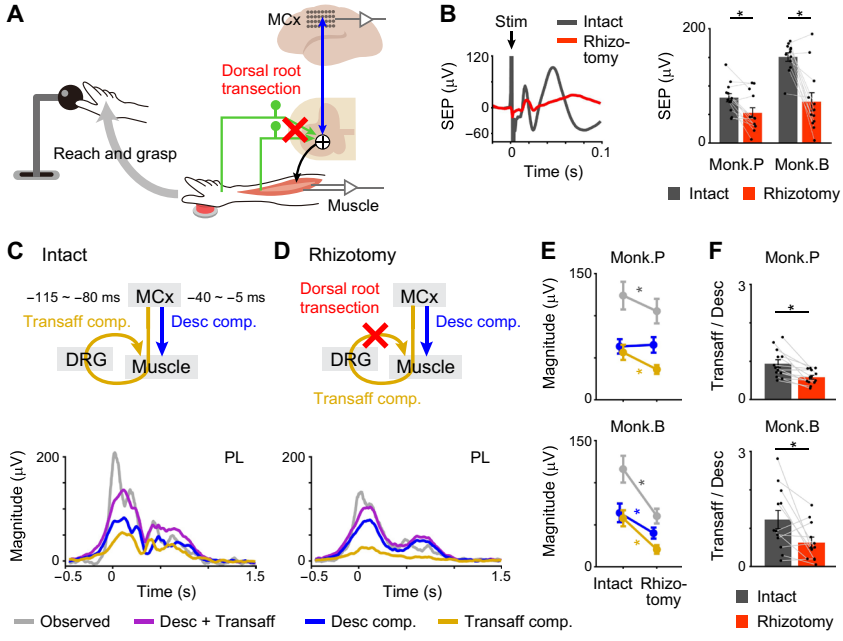

Fig. 7. Sectioning of peripheral afferents impairs the transafferent activation of muscles by MCx. (**A**) Experimental setup. (**B**) Left: Example of somatosensory evoked potentials (SEPs) elicited by electrical stimulation of a forelimb muscle (EDC). Right: Sizes of SEPs recorded over the primary somatosensory cortex (monkey P, 13 muscles; and monkey B, 12 muscles). (**C**) The observed muscle activity, its reconstruction using descending and transafferent inputs, and each subcomponent aligned to movement onset before dorsal rhizotomy. (**D**) Same as in (C), but after dorsal rhizotomy. (**E**) Total muscle activity (gray) and size of descending (blue) and transafferent (yellow) components before and after dorsal rhizotomy. The muscle activity and the sizes of descending and transafferent components after dorsal rhizotomy were compared to those observed before dorsal rhizotomy (monkey P, 13 muscles; and monkey B, 12 muscles). (**F**) Ratio of the size of the transafferent component to that of the descending component was compared before and after dorsal rhizotomy (monkey P, 13 muscles; and monkey B, 12 muscles). In (B), (E), and (F), data are the means ± SEM. $^*P < 0.05$, paired two-tailed t test. P values are described in tables S8 to S10.

(12 muscles), intact = 59.1 ± 9.8 and rhizotomy = 21.2 ± 5.1; Fig. 7, C to E]. This result demonstrated that dorsal rhizotomy impaired signal transmission from M1 through the transafferent pathway, which usually activates muscles in intact animals. On the other hand, the size of the descending component remained after dorsal rhizotomy in monkey P (intact = 63.5 ± 8.6 and rhizotomy = 65.4 ± 9.2; Fig. 7E). Furthermore, the ratio of the size of the transafferent component to that of the descending component decreased after dorsal rhizotomy in monkeys P and B [monkey P (13 muscles), intact = 0.94 ± 0.10 and rhizotomy = 0.59 ± 0.05; and monkey B (12 muscles), intact = 1.23 ± 0.24 and rhizotomy = 0.63 ± 0.14; Fig. 7F], indicating that the decrease in the transafferent component size cannot be explained by the decrease in the descending component size alone. These results provide causal evidence that M1 signals transmitted through the transafferent pathway are involved in the activation of forelimb muscles during voluntary movements.

DISCUSSION

Elucidation of how supraspinal and spinal structures in the nested hierarchy control limb muscles represents a critical inquiry in the neural control of limb movements. Historically, a range of theories, including the servo control hypothesis (*23*), the equilibrium-point hypothesis (*33*, *34*), and the internal model for motor control (*24*), have been proposed to incorporate the concept of spinal reflexes into cortical control of limb movements. More recently, theoretical frameworks such as the optimal feedback control theory (*35*, *36*) and active inference (*25*) have been developed to deepen our understanding of the neural control of limb movements, particularly in explaining adaptive behaviors in response to unexpected external changes. Despite these theoretical advancements, the specific neural mechanism through which the central nervous system, in concert with spinal reflexes, orchestrates motor control signals, particularly concerning the flow of information encoded in neural activities across sensorimotor circuits, remains elusive (*37*).

To address this problem, our study involved extensive recordings from MCx, peripheral afferents, and forelimb muscles of monkeys performing a reach-to-grasp movement. We have previously elucidated the integration process of descending and sensory inputs within the spinal cord during voluntary movements (*21*). The current study further explored how the nested hierarchy encompassing MCx and spinal structures coordinates limb movements and provides insights into the neural mechanisms of motor control by M1. We particularly focused on investigating the information transmitted from M1 to muscles through the transafferent pathway. Our findings demonstrated that M1 influences muscle activity not only through direct activation via the descending pathway but also through delayed activation via the transafferent pathway (as shown in fig. S9). Therefore, to ensure precise control of limb muscles through these two distinct pathways, which operate on different time scales, M1 generates appropriate motor output based on an internal forward model that anticipates upcoming spinal reflexes.

Multiple pathways exist for signals to travel from M1 to peripheral afferents. The most relevant time difference between M1 and afferent activity was 75 ms (Fig. 2D). On the basis of the assumption that afferent activity is induced by the activation of limb muscles in approximately 50 ms (*38*), it is likely that the activation of alpha motor neurons and ensuing limb movements lead to afferent activity, including signals from cutaneous receptors in the skin and proprioceptors in muscles, tendons, and joints. Muscle contraction also triggers Golgi tendon organ activation. In addition, afferent activity was detected around the time of movement onset (Fig. 1C), possibly resulting from the gamma efferent drive leading to muscle spindle activation. The strong relationship between M1 and peripheral afferents of various modalities could underlie the encoding of the transafferent activation of muscles by M1.

The activity of peripheral afferents could be transmitted to muscles through the transcortical pathway, often referred to as the "transcortical reflex" pathway (*39*). This signaling pathway is critical for adaptive motor control. In primates, peripheral afferent signals activated by a sudden stretch of forelimb muscles are postulated to be conveyed to these muscles within 50 ms via the transcortical pathway (*40*). Concurrently, the fastest response time of peripheral afferent activity from limb movements is approximately 10 ms in monkeys (*41*), indicating that there is an estimated 10 ms delay from stretch to peripheral afferent activity. This results in a conduction delay of approximately 40 ms from peripheral afferent activity to muscle activation through the transcortical pathway. Similarly, sensory nerve activation by electrical stimulation in monkeys modulates muscle activity at 50 ms via the transcortical pathway (*42*). Consequently, we set a cutoff delay of 40 ms for the influence of afferents on muscles to exclude effects mediated by the transcortical pathway, suggesting that most afferent effects on muscles are due to spinal reflex pathways. In addition, the information transmitted from peripheral afferents to M1 through the transcortical reflex pathway would be surely embedded in M1 activity analyzed in our study. Together, our predictive model for muscle activity incorporates the transcortical reflex component in addition to the short reflex component through the spinal reflex pathway.

Descending motor signals from supraspinal structures modulate peripheral afferent inputs to alter the feedback gain of spinal sensory transmission in a state-dependent manner, notably through presynaptic inhibition (*43*). Genetic ablation of presynaptic inhibition leads to the loss of smooth reaching movements and aberrant oscillatory movements (*44*). These abnormal movements are detected only after the onset of reaching, which suggests that the modulated afferent inputs predominantly affect muscle activity after the reaching movement. These results correspond with our findings that afferent components are mainly detected after movement onset. Presumably, presynaptic inhibition is controlled by descending cortical signals (*45*, *46*) and its involvement cannot be excluded; however, our analysis did not consider adjustments for the gain of afferent inputs because we used a linear model. Investigating this gain modulation of afferent inputs requires recording afferent activities in more complex tasks, such as comparisons between active movements and resting states. If recording techniques are improved in the future to enable long-term stable recording of neuronal activity, including peripheral afferents, while animals perform multiple tasks and for longer periods, we can evaluate whether M1 anticipates cortical modulation of the spinal reflex during reaching movements.

Direct corticospinal projections from M1 in primates are the densest and most numerous among motor-related cortical areas (*47*). In addition, the most notable feature in M1 of macaque monkeys is the presence of direct connections from pyramidal neurons in M1 to spinal motor neurons, which exert a strong impact on muscle activity (*20*, *48*–*52*). It is therefore widely assumed that these robust descending control signals from M1 act on spinal motor neurons to produce the appropriate muscle activity required to execute

the intended movement (*6*). Our study demonstrated that M1 primarily encoded muscle activity driven by transafferent pathways during movements (Fig. 6 and figs. S5 and S8), which decreased after sectioning dorsal roots at the cervical segments (Fig. 7, C to F). These findings suggest that the impact of M1 on spinal motor neurons, resulting muscle activation and limb movement, further activates spinal reflexes.

Dorsal rhizotomy reduced muscle activity and the transafferent component (Fig. 7, C to F, and fig. S7A). Figure 1B shows the tonic firing of some peripheral afferents, which may maintain spinal cord excitability. This finding raises the possibility that dorsal rhizotomy might lead to a reduction in this excitability. On the other hand, an increase in the hypersensitivity of spinal neurons following deafferentation has been reported (*53*). In any case, the reduction in the transafferent component was markedly greater than that in the descending component after dorsal rhizotomy in both animals (Fig. 7F). This observation lends support to the idea that these alterations cannot be solely ascribed to the reduced influence of direct projections, but dorsal rhizotomy predominantly affects the transafferent component. These findings suggest that spinal reflexes amplify the direct descending commands from M1 under intact conditions. Hence, M1 minimizes cortical energy expenditure by leveraging the spinal reflex system to control limb muscles adequately. This efficient control of limb muscles by M1 is consistent with the theory of optimal feedback control, a leading theoretical framework in motor control that computes the optimal strategy for reducing movement error and motor effort (*35*, *54*). According to this theory, the control policy provides feedforward motor commands to the spinal motor neurons based on the estimated current state and task demands. MCx, brainstem, and peripheral afferents projecting to spinal motor neurons are assumed to be the brain regions responsible for the control policy (*55*). How the distributed organization of the control policy controls the end effectors has not been fully understood yet (*9*). The current study showed that during voluntary limb movements, M1 sends motor outputs based on a predictive model of sensorimotor integration in the spinal cord, providing evidence for the neuronal mechanism underlying the interplay between M1 and peripheral afferents. Incorporating spinal model implementation by M1 into a theory for movement control will help us to clarify how the central nervous system controls voluntary limb movements.

Limitations

Conventional analyses of stretch reflexes focus on muscle responses to perturbations at specific joints (*18*). Our study extended this approach by exploring muscle activity components influenced by peripheral afferent inputs or transafferent inputs from M1 during single-joint movements at the onset of a reaching movement (Fig. 5 and fig. S4). Intriguingly, muscle spindle activity has been observed during slower movements, such as ramp and hold movements, suggesting that afferent input may also be transmitted to spinal motor neurons during such slower movements (*56*). Consequently, interpreting afferent or transafferent components in the context of stretch reflexes and reciprocal inhibition aligns with established methodologies in stretch reflex analysis, even though our experiment does not assess these components across varying stretch magnitudes as in conventional analyses. Because spontaneous movements cannot be constrained in awake monkeys, it was very difficult to accurately identify the sensory receptors of the recorded afferents in awake monkeys, as had been attempted in the previous study (*57*). Whether the peripheral afferent signals induced by a stretched muscle during voluntary limb movements are transmitted back to the same stretched muscle or to its antagonist muscle is an important question for future research.

MATERIALS AND METHODS

Experimental design

We hypothesized that the output from MCx might produce subsequent afferent activity, which could then further influence muscles through the transafferent pathway with a delay. To examine this hypothesis, we analyzed the data in simultaneous recordings of the activities in MCx, forelimb muscles, and an ensemble of afferent neurons in two behaving monkeys (*21*). We further investigate whether selective blockade of the transafferent pathway would lead to reduced muscle activity, particularly its transafferent component, by conducting dorsal rhizotomy at the C6-C8 levels in two additional monkeys. The current study has been posted on the preprint server (*58*, *59*).

Animals

We used one adult male monkey (monkey T, weight of 6 to 7 kg, *Macaca fuscata*) and three adult female monkeys (monkey C, weight of 5 to 6 kg, *Macaca mulatta*; monkey P, weight of 4 to 5 kg, *Macaca fuscata*; and monkey B, weight 5 to 6 kg, *Macaca fuscata*). The experiments were approved by the Experimental Animal Committee of the National Institute of Natural Sciences (11A157, 12A139, 13A119, 14A116, and 15A068) and Tokyo Metropolitan Institute of Medical Science (20-053, 21-048). The animals were cared for and treated humanely in accordance with *National Institutes of Health Guidelines*. Part of the dataset obtained from monkeys T and C is the same as the dataset used in our previous studies (*21*, *26*).

Surgery

All surgical procedures were performed using sterile techniques while the animal was anesthetized with 1 to 2% isoflurane (monkeys T and C) or sevoflurane (monkeys P and B). Dexamethasone, atropine, and ampicillin were administered preoperatively; ampicillin and ketoprofen were given postoperatively.

For EMG recordings, we implanted pairs of Teflon-insulated wire electrodes (AS631; Cooner Wire) into the forelimb muscles on the right side. We evaluated the activity in the deltoideus posterior (Del), triceps brachii (Tri), biceps brachii (Bi), brachioradialis (BR), extensor carpi radialis (ECR), flexor carpi radialis (FCR), flexor carpi ulnaris (FCU), extensor digitorum communis (EDC), palmaris longus (PL), flexor digitorum superficialis (FDS), abductor pollicis longus (APL), and adductor pollicis (AP) of monkey T; the Del, triceps brachii longus (TriLo), TriLa, BR, ECR, FCU, EDC, flexor digitorum profundus (FDP), APL, and AP of monkey C; the Del, Tri, Bi, BR, ECR, ECU (extensor carpi ulnaris), FCU, EDC, ED23 (extensor digitorum-2,3), ED45 (extensor digitorum-4,5), PL, FDS, and FDP of monkey P; and the Del, Tri, Bi, BR, ECR, FCR, ECU, EDC, ED23, PL, FDS, and AP of monkey B.

To record ECoG signals from MCx, we implanted a 32-channel (monkeys T and C) or 30-channel (monkeys P and B) grid electrode array (Unique Medical) with a diameter of 1 mm and an interelectrode distance of 3 mm beneath the dura mater over the sensorimotor cortex (figs. S5B and S8B). We placed the ground and reference electrodes over the ECoG electrode so that they contacted the dura. To record afferent signals, we implanted two multielectrode arrays

(Blackrock Neurotech) into the dorsal root ganglia at the cervical level (monkey T, C7 and C8; and monkey C, C6 and C7) on the right side. To block peripheral afferent inputs, we sectioned the cervical dorsal rootlets (dorsal rhizotomy) at segments C6-C8 (*60*, *61*).

Behavioral task

All monkeys were operantly conditioned to perform a reach-to-grasp task with the right hand (Figs. 1A and 7A). After putting its hand on a home button for 2 to 2.5 s (monkeys T and C) or 1 s (monkeys P and B), the monkey reached for a lever and pulled it to receive a reward.

Recordings

All neural and muscular signals were recorded simultaneously using a data acquisition system (Plexon for monkeys T and C and Tucker-Davis Technologies for monkeys P and B). EMG signals were amplified using amplifiers (AB-611J; Nihon Kohden); they were sampled at 2000 Hz in monkey T and at 1000 Hz in monkey C at a gain of ×1000 to 2000 and sampled at 1017.3 Hz in monkeys P and B at a gain of ×100. We applied a second-order Butterworth bandpass filter (1.5 to 60 Hz) to the signals, rectified the filtered signals, resampled the signals to 200 Hz, and smoothed the resampled signals using a moving window of 11 bins.

The ECoG signals of monkeys T and C were amplified using a multichannel amplifier (Plexon MAP system; Plexon) at a gain of ×1000 and sampled at 2000 Hz in monkey T and at 1000 Hz in monkey C. The ECoG signals of monkeys P and B were amplified using a multichannel amplifier (PZ2; Tucker-Davis Technologies) at a gain of ×51 and sampled at 1017.3 Hz. We applied a second-order Butterworth bandpass filter (1.5 to 240 Hz) to the signals, computed a short-time fast Fourier transform on moving 100-ms windows of the filtered signals at a 5-ms step, normalized the power to the average power in each session, and calculated the average power in the high-gamma bands (high-gamma 1, 60 to 120 Hz; and high-gamma 2, 120 to 180 Hz). We considered the high-gamma power of the ECoG signals to be representative of neural activity in cortical areas (*27*).

The peripheral afferent activities of monkeys T and C were initially amplified at a gain of ×20,000 and sampled at 40 kHz (Plexon MAP system; Plexon). We extracted filtered waves (150 to 8000 Hz) above an amplitude threshold, sorted the thresholded waves using semiautomatic sorting methods (Offline Sorter; Plexon), and performed manual verification. We isolated 25 to 39 units in monkey T and 11 to 15 units in monkey C. We convolved the inversion of the interspike interval using an exponential decay function whose time constant was 50 ms and resampled the firing rate to 200 Hz.

We calculated the movement-related modulation of the EMG signals, the ECoG signals, and the peripheral afferent activity before analyzing the data. We first calculated the baseline activity by averaging the activity from −1250 to −750 ms around movement onset. We then subtracted the baseline activity from the preprocessed activity. We used movement-related modulation throughout the premovement and movement periods (−500 to 1500 ms around movement onset) for monkeys T, C, and P as a single trial for further analysis. Since monkey B could reach the lever but did not grasp it after dorsal rhizotomy, we used movement-related modulation throughout the premovement and movement periods (−500 to 250 ms around movement onset) for monkey B. We recorded the times at which the animals released the home button, pulled the lever, and pushed the home button.

We recorded the forelimb movements of monkeys T and C using an optical motion capture system with 12 cameras (Eagle-4, Motion Analysis). The spatial positions of 10 reflective markers attached to the surface of the forelimbs and body were sampled at 200 Hz.

We assessed the sectioning of peripheral afferents by recording SEPs over the primary somatosensory cortex elicited by electrical stimulation (2 mA, 200 monophasic pulses of 1 ms width at 2.42 Hz) of the forelimb muscles of monkeys P and B under anesthesia with ketamine, xylazine, and atropine. The forelimb muscles were stimulated using subcutaneously implanted wire electrodes intended for EMG recordings (2 mA, 200 monophasic pulses with a 1 ms width at 2.42 Hz). SEPs were recorded using the same electrodes used for ECoG recording. The signals were amplified using a multichannel amplifier (PZ2; Tucker-Davis Technologies) at a gain of ×51 and sampled at 1017.3 Hz. To calculate the SEP size, we subtracted the minimum value that was recorded between 11 and 20 ms after stimulation by any of the electrodes over the primary somatosensory cortex from the maximum value that was recorded between 16 and 25 ms after stimulation.

Sparse linear regression

Neural ensemble activity in M1 satisfactorily accounts for muscle activity when a linear model is used (*62*, *63*). We examined whether the integration of the descending signals from M1 and somatosensory signals from peripheral afferents in spinal motor neurons can also be represented as a linear relationship. We modeled muscle activity as a weighted linear combination of high-gamma activity in MCx and/or neuronal activity of peripheral afferents using multidimensional linear regression as follows

$$y_{j,T}(t) = \sum_{k,l} w_{j,k,l} \times x_{k,T}(t + l\delta) \quad (1)$$

where $y_{j,T}(t)$ is a vector of the EMG activity of muscle j (12, 10, 13, and 12 muscles for monkeys T, C, P, and B, respectively) at time index t in trial T, $x_{k,T}(t + l\delta)$ is an input vector of the peripheral afferent or cortical signal k at time index t and lag time $l\delta$ ($\delta = 5$ ms and $l = -8$ to -1) in trial T, and $w_{j,k,l}$ is a vector of weights on the peripheral afferent or cortical signal k at lag time $l\delta$. We applied a Bayesian sparse linear regression algorithm that introduces sparse conditions for the unit/channel dimension (*64*). This algorithm implements the Variational Bayesian method with Automatic Relevance Determination prior. The algorithm selects an optimal model parameter based on the data and introduces sparseness for the inputs to suppress the overfitting problem. As we examined how the combined activity in MCx and/or peripheral afferents influenced subsequent muscle activity, lag time $l\delta$ (Eq. 1) was set to negative values. To represent the effect of peripheral afferents on muscle activity (afferent input), we used the activity in the peripheral afferents from −40 to −5 ms (8 bins of 5 ms each) to reconstruct muscle activity at time 0 for the following reasons. Averaging the muscle activity triggered at the spiking activity of peripheral afferents showed postspike facilitation with a latency of 5.8 ms (*57*). Thus, we set 5 ms as the shortest lag time. In addition, the delay time in the reflex pathways was reported to be 47 ms (*65*). Afferent signals are transmitted to the muscle not only through the spinal reflex pathway but also via the transcortical reflex pathway (*39*). However, since MCx is involved in the transcortical reflex pathway, its effects on muscle activity are already incorporated into the linear model under MCx component. To avoid double-counting these effects, it was necessary to exclude

the influence of afferent activity via the transcortical reflex pathway when constructing the linear models. Previous studies in both humans and monkeys have shown that the latency via the transcortical reflex pathway is approximately 50 ms (*40*, *66*). In our prior study, we used this 50-ms time frame as the cutoff delay (*21*). However, the referenced studies (*40*, *66*) measured the latency from hand perturbation to muscle activity which including the delay from mechanical perturbation to activation of mechanoreceptors, while our analysis focused on the time it takes for afferent activity to be transmitted to muscles via the transcortical reflex pathway. Given that the fastest response time of peripheral afferent activity from limb movements is approximately 10 ms in monkeys (*41*), we estimated a 10-ms delay from the initial stretch to the onset of afferent activity. This led us to infer a conduction delay of approximately 40 ms from peripheral afferent activity to muscle activation through the transcortical reflex pathway. Similarly, in monkeys, sensory nerve activation by electrical stimulation modulates muscle activity within 50 ms via this pathway (*42*). Consequently, in the current study, we set a cutoff delay of 40 ms to focus on the effects of afferents on muscles that are not mediated by the transcortical reflex pathway, suggesting that most afferent effects on muscles likely mediated by spinal reflex pathways. To represent the reafferent effect of MCx on muscle activity through the transafferent pathway composed of descending and spinal reflex pathways (transafferent input), we used the activity in MCx from −80 to −115 ms (eight bins of 5 ms each) to reconstruct muscle activity at time 0. We obtained this lag time by simply adding the time at which MCx most accurately accounted for the peripheral afferent activity (75 ms) to the lag time of the descending input. To represent the direct effect of MCx on muscle activity through the descending pathway (descending input), we used activity in MCx from −40 to −5 ms (eight bins of 5 ms each) to reconstruct muscle activity at time 0 for the following reasons. Averaging the muscle activity triggered at the spiking activity of M1 neurons shows post-spike facilitation with a latency of 6.7 ms (*48*). Accordingly, we set 5 ms as the shortest lag time. The weighted sum of M1 neuronal activity accurately accounted for muscle activity at a lag time of 40 to 60 ms (*67*). However, it is possible that MCx has some effect on muscle activity through the somatic reflex arc within 75 ms, as shown in Fig. 2D. To avoid the influence of the somatic reflex arc, we set 40 ms as the longest lag time.

To compute the contribution of each descending, afferent, and transafferent input to the reconstruction of muscle activity, we calculated each subcomponent of the reconstructed activity using the relevant input and the respective weight values in a decoding model built from the combined inputs. For example, the descending component was calculated as follows

$$y\_\mathrm{Desc}_{j,T}(t) = \sum_{k,l} w_{j,k,l} \times x\_\mathrm{Desc}_{k,T}(t + l\delta) \quad (2)$$

where $y\_\mathrm{Desc}_{j,T}(t)$ is a vector of the descending component at muscle j at time index t in trial T, $x\_\mathrm{Desc}_{k,T}(t + l\delta)$ is an input vector of the cortical signal k at time index t and lag time $l\delta$ in trial T, and $w_{j,k,l}$ is derived from a vector of weights in Eq. 1 but with the weights assigned to peripheral afferents removed. We also calculated subcomponents from the activity in each single afferent, each cortical area, or each electrode in a similar way.

The activity of peripheral afferents was modeled as a weighted linear combination of MCx activity using multidimensional linear regression as follows

$$y_{j,T}(t + Tpred) = \sum_{k,l} w_{j,k,l} \times x_{k,T}(t + l\delta) \quad (3)$$

where $y_{j,T}(t)$ is a vector of the peripheral afferent j at time index t in trial T, $x_{k,T}(t + l\delta)$ is an input vector of the cortical signal k at time index t and lag time $l\delta$ ($\delta = 5$ ms and $l = -8$ to -1) in trial T, and $w_{j,k,l}$ is a vector of weights on the cortical signal k at lag time $l\delta$. We considered that MCx activity evokes muscle activity that then generates peripheral afferent activity. We set the lag time $l\delta$ to negative values. By changing *Tpred* from 0 to 120 ms, we identified *Tpred*, the time point at which the reconstruction accuracy of the activity in peripheral afferents was the highest (75.0 ms, with an average of 66.6 ms for monkey T and 83.4 ms for monkey C; Fig. 2D).

Data analysis

We analyzed data from 21 and 7 sessions, each of which was 10 min, for monkeys T and C, respectively (table S26). The movement times of monkeys P and B increased temporarily after dorsal rhizotomy. To compare the magnitude of muscle activity without the bias from differences in movement time, we used trials in which the monkeys performed the movement within a certain period (0.65 to 0.85 s for the movement time of monkey P and 0.13 to 0.19 s for the reach time of monkey B) based on the distribution of movement or of reach time observed for these animals in the intact condition (fig. S6A). We divided the data into datasets that included no fewer than 129 trials (see below). For monkey P, we analyzed the data from 17 and 4 sessions before and after dorsal rhizotomy, respectively; for monkey B, we analyzed the data from 8 and 2 sessions before and after dorsal rhizotomy, respectively (table S26). We used data obtained up to 5 days after dorsal rhizotomy to examine the acute effect of dorsal rhizotomy without the reorganization of neural circuits.

We constructed models designed to reconstruct the temporal changes in the EMG signals or afferent activity using a partial dataset (training dataset) and tested them using the remainder of the same dataset (test dataset). One hundred and eight trials were randomly selected as a training dataset, and 21 trials were randomly selected from the remaining trials as the test dataset. To assess the model, we calculated the correlation coefficients between the observed data and their reconstructions in the test dataset. We also calculated the VAF as follows

$$\mathrm{VAF} = 1 - \frac{\sum \left[y(t) - f(t)\right]^2}{\sum \left[y(t) - \overline{y(t)}\right]^2} \quad (4)$$

where $y(t)$ is a vector of the actual activity in muscles at time index t, $\overline{y(t)}$ is the mean of $y(t)$, and $f(t)$ is the reconstructed activity at time index t. We performed sixfold cross-validation in the analysis of each session and used averaged values for the analysis. We then calculated the average activity of each muscle or peripheral afferent using data taken from 21 (monkey T), 7 (monkey C), 17 (monkey P, before rhizotomy), 4 (monkey P, after rhizotomy), 8 (monkey B, before rhizotomy), or 2 (monkey B, after rhizotomy) sessions. In control analyses of the model reconstruction, we created surrogate training datasets in which we shuffled the temporal profiles of the inputs independently across different blocks to generate a model, and we subsequently calculated the reconstruction using actual data to evaluate the model (Fig. 2, B and C; and figs. S2, B and C, and S7, B and C) or shuffled data to evaluate the inputs (Fig. 4, E, F, and I; and figs. S3, C and D, and S4). We also used MCx activity occurring

5 to 40 ms after the muscle activity to be calculated as another control dataset for evaluation of transafferent inputs (Fig. 4, E, F, and I; and figs. S3, E and F, and S4).

We observed a period in which there was movement-related modulation of muscles. To obtain the onset time of the observed muscle activity, we first calculated the average of the aligned waveforms in the test dataset. We then defined one-fifth of the maximum amplitude of the observed muscle activity from 250 ms before to 250 ms after movement onset as a threshold. If the activity or the reconstruction exceeded the threshold in five consecutive bins, the first of these bins was set as the onset. We calculated the average onset values observed in six test datasets in one session and obtained their average values over all sessions. To obtain the offset time, we calculated the average of the aligned waveforms of the muscle activity and analyzed the data obtained 500 ms after the onset of movement. If the averaged data values were below the same threshold used to calculate the onset time in five consecutive bins, the first of these bins was set as the offset. The calculated onset and offset corresponded well with those determined by visual inspection. We calculated the area above or below baseline for each component during the period in which movement-related modulation of muscles was detected (monkey T, −100 to 1150 ms around movement onset; monkey C, −100 to 1300 ms; and monkey P, −200 to 800 ms) and from the time of onset of muscle activity to the time the animal reached the lever (monkey B, −300 to 150 ms) (Figs. 4, B and D, and 7, E and F; and fig. S3, B, D, and F). We similarly calculated the sum of the areas above and below baseline for each component from each cortical area and each electrode during these periods and normalized them to the values from the whole area (Fig. 6, C and D, and figs. S5 and S8). Then, we divided these areas by the time of movement-related modulation of muscles. We calculated the firing rate of afferents and that of each component from each cortical area and each electrode during the period in which movement-related modulation of muscles was detected (monkey T, −100 to 1150 ms around movement onset; and monkey C, −100 to 1300 ms) and divided the values by the duration of movement-related modulation of muscles (Fig. 6, C and D, and fig. S5). We tested whether the positive or negative values deviated from zero using a standard *t* test. The time at which the wrist joint angle initially peaked along the flexion/extension direction of monkey T was 51.4 ± 9.6 ms (mean ± SD), and the time at which the wrist joint angle initially peaked along the flexion/extension direction and at which the elbow joint angle initially peaked along the pronation/supination direction of monkey C were 31.4 ± 5.6 ms and 47.1 ± 2.7 ms, respectively (Fig. 5A). We calculated the temporal mean of each component during the period from the beginning of the reaching movement (from 55 to 100 ms around movement onset) (Fig. 5C and fig. S4). We statistically tested whether the temporal mean deviated from zero using a standard *t* test.

Using a linear model, we obtained the lag time between afferents and MCx activity at which the afferent activity was most accurately reconstructed from MCx activity. We first selected data for which the correlation coefficient or VAF of the model was superior to that of models built using a surrogate shuffled control. We then created a graph of the relationship between the lag time and reconstruction accuracy using only the data that led to high accuracy (correlation coefficient greater than 0.4 and VAF greater than 0.15). We fitted a quadratic function to the graph and obtained the vertex of the fitting curve.

Statistical analysis

We used the paired or unpaired Student's *t* test. When comparing more than two group means, we first assessed the data using one-way analysis of variance (ANOVA). The alpha level of significance was set at 0.05. The results of all the statistical tests (including *P* values) are included in Supplementary Tables. The data are expressed as the mean ± SEM or the mean ± SD. We used MATLAB R2020a (MathWorks) for statistical analysis. No statistical methods were used to predetermine the sample size. However, the sample sizes followed published standards.

Supplementary Materials

This PDF file includes:

Figs. S1 to S9

Tables S1 to S26

REFERENCES AND NOTES

1. J. Merel, M. Botvinick, G. Wayne, Hierarchical motor control in mammals and machines. *Nat. Commun.* **10**, 5489 (2019).
2. D. J. Felleman, D. C. Van Essen, Distributed hierarchical processing in the primate cerebral cortex. *Cereb. Cortex* **1**, 1–47 (1991).
3. A. B. Schwartz, Useful signals from motor cortex. *J. Physiol.* **579**, 581–601 (2007).
4. R. N. Lemon, Descending pathways in motor control. *Annu. Rev. Neurosci.* **31**, 195–218 (2008).
5. B. Alstermark, T. Isa, Circuits for skilled reaching and grasping. *Annu. Rev. Neurosci.* **35**, 559–578 (2012).
6. J. F. Kalaska, From intention to action: Motor cortex and the control of reaching movements. *Adv. Exp. Med. Biol.* **629**, 139–178 (2009).
7. M. Omrani, M. T. Kaufman, N. G. Hatsopoulos, P. D. Cheney, Perspectives on classical controversies about the motor cortex. *J. Neurophysiol.* **118**, 1828–1848 (2017).
8. K. V. Shenoy, M. Sahani, M. M. Churchland, Cortical control of arm movements: A dynamical systems perspective. *Annu. Rev. Neurosci.* **36**, 337–359 (2013).
9. A. B. Schwartz, Movement: How the brain communicates with the world. *Cell* **164**, 1122–1135 (2016).
10. M. M. Churchland, J. P. Cunningham, M. T. Kaufman, J. D. Foster, P. Nuyujukian, S. I. Ryu, K. V. Shenoy, Neural population dynamics during reaching. *Nature* **487**, 51–56 (2012).
11. M. T. Kaufman, M. M. Churchland, S. I. Ryu, K. V. Shenoy, Cortical activity in the null space: Permitting preparation without movement. *Nat. Neurosci.* **17**, 440–448 (2014).
12. J. M. Donelan, K. G. Pearson, Contribution of sensory feedback to ongoing ankle extensor activity during the stance phase of walking. *Can. J. Physiol. Pharmacol.* **82**, 589–598 (2004).
13. J. B. Nielsen, T. Sinkjaer, Afferent feedback in the control of human gait. *J. Electromyogr. Kinesiol.* **12**, 213–217 (2002).
14. T. Sinkjaer, J. B. Andersen, M. Ladouceur, L. O. Christensen, J. B. Nielsen, Major role for sensory feedback in soleus EMG activity in the stance phase of walking in man. *J. Physiol.* **523**, 817–827 (2000).
15. T. R. Nichols, Distributed force feedback in the spinal cord and the regulation of limb mechanics. *J. Neurophysiol.* **119**, 1186–1200 (2018).
16. J. B. Nielsen, Human spinal motor control. *Annu. Rev. Neurosci.* **39**, 81–101 (2016).
17. E. Jankowska, Interneuronal relay in spinal pathways from proprioceptors. *Prog. Neurobiol.* **38**, 335–378 (1992).
18. H. Hultborn, Spinal reflexes, mechanisms and concepts: From Eccles to Lundberg and beyond. *Prog. Neurobiol.* **78**, 215–232 (2006).
19. J. Kalambogias, Y. Yoshida, Converging integration between ascending proprioceptive inputs and the corticospinal tract motor circuit underlying skilled movement control. *Curr. Opin. Physio.* **19**, 187–193 (2021).
20. E. E. Fetz, P. D. Cheney, D. C. German, Corticomotoneuronal connections of precentral cells detected by postspike averages of EMG activity in behaving monkeys. *Brain Res.* **114**, 505–510 (1976).
21. T. Umeda, T. Isa, Y. Nishimura, Temporal dynamics of the sensorimotor convergence underlying voluntary limb movement. *Proc. Natl. Acad. Sci. U.S.A.* **119**, e2208353119 (2022).
22. J. A. Pruszynski, I. Kurtzer, T. P. Lillicrap, S. H. Scott, Temporal evolution of "automatic gain-scaling". *J. Neurophysiol.* **102**, 992–1003 (2009).
23. P. Merton, A., in *The Spinal Cord*. (Wiley, 1953), chap. 183–198.
24. M. Kawato, D. Wolpert, Internal models for motor control. *Novartis Found. Symp.* **218**, 291–304 (1998).

25. R. A. Adams, S. Shipp, K. J. Friston, Predictions not commands: Active inference in the motor system. *Brain Struct. Funct.* **218**, 611–643 (2013).
26. T. Umeda, T. Isa, Y. Nishimura, The somatosensory cortex receives information about motor output. *Sci. Adv.* **5**, eaaw5388 (2019).
27. S. Ray, S. S. Hsiao, N. E. Crone, P. J. Franaszczuk, E. Niebur, Effect of stimulus intensity on the spike-local field potential relationship in the secondary somatosensory cortex. *J. Neurosci.* **28**, 7334–7343 (2008).
28. C. Capaday, C. van Vreeswijk, Linear summation of outputs in a balanced network model of motor cortex. *Front. Comput. Neurosci.* **9**, 63 (2015).
29. C. Ethier, L. Brizzi, W. G. Darling, C. Capaday, Linear summation of cat motor cortex outputs. *J. Neurosci.* **26**, 5574–5581 (2006).
30. E. Todorov, Direct cortical control of muscle activation in voluntary arm movements: A model. *Nat. Neurosci.* **3**, 391–398 (2000).
31. Y. Q. Jiang, B. Zaaimi, J. H. Martin, Competition with primary sensory afferents drives remodeling of corticospinal axons in mature spinal motor circuits. *J. Neurosci.* **36**, 193–203 (2016).
32. C. Darian-Smith, A. Lilak, C. Alarcón, Corticospinal sprouting occurs selectively following dorsal rhizotomy in the macaque monkey. *J. Comp. Neurol.* **521**, 2359–2372 (2013).
33. A. G. Fel'dman, On the functional tuning of the nervous system in movement control or preservation of stationary pose. II. Adjustable parameters in muscles. *Biofizika* **11**, 498–508 (1966).
34. A. G. Feldman, Once more on the equilibrium-point hypothesis (lambda model) for motor control. *J. Mot. Behav.* **18**, 17–54 (1986).
35. S. H. Scott, Optimal feedback control and the neural basis of volitional motor control. *Nat. Rev. Neurosci.* **5**, 532–545 (2004).
36. E. Todorov, M. I. Jordan, Optimal feedback control as a theory of motor coordination. *Nat. Neurosci.* **5**, 1226–1235 (2002).
37. G. E. Loeb, Learning to use muscles. *J. Human Kinet.* **76**, 9–33 (2021).
38. A. B. Vallbo, Discharge patterns in human muscle spindle afferents during isometric voluntary contractions. *Acta Physiol. Scand.* **80**, 552–566 (1970).
39. C. Capaday, R. Forget, R. Fraser, Y. Lamarre, Evidence for a contribution of the motor cortex to the long-latency stretch reflex of the human thumb. *J. Physiol.* **440**, 243–255 (1991).
40. J. A. Pruszynski, I. Kurtzer, J. Y. Nashed, M. Omrani, B. Brouwer, S. H. Scott, Primary motor cortex underlies multi-joint integration for fast feedback control. *Nature* **478**, 387–390 (2011).
41. M. T. Jahnke, A. Struppler, Response of human muscle spindle afferents to abrupt load perturbations. *Brain Res.* **501**, 324–331 (1989).
42. D. G. Rüegg, M. Chofflon, Peripheral and transcortical loops activated by electrical stimulation of the tibial nerve in the monkey. *Exp. Brain Res.* **50**, 293–298 (1983).
43. E. Azim, K. Seki, Gain control in the sensorimotor system. *Curr. Opin. Physio.* **8**, 177–187 (2019).
44. A. J. Fink, K. R. Croce, Z. J. Huang, L. F. Abbott, T. M. Jessell, E. Azim, Presynaptic inhibition of spinal sensory feedback ensures smooth movement. *Nature* **509**, 43–48 (2014).
45. S. Tomatsu, G. Kim, S. Kubota, K. Seki, Presynaptic gating of monkey proprioceptive signals for proper motor action. *Nat. Commun.* **14**, 6537 (2023).
46. K. Seki, S. I. Perlmutter, E. E. Fetz, Sensory input to primate spinal cord is presynaptically inhibited during voluntary movement. *Nat. Neurosci.* **6**, 1309–1316 (2003).
47. K. Toyoshima, H. Sakai, Exact cortical extent of the origin of the corticospinal tract (CST) and the quantitative contribution to the CST in different cytoarchitectonic areas. A study with horseradish peroxidase in the monkey. *J. Hirnforsch.* **23**, 257–269 (1982).
48. E. E. Fetz, P. D. Cheney, Postspike facilitation of forelimb muscle activity by primate corticomotoneuronal cells. *J. Neurophysiol.* **44**, 751–772 (1980).
49. J. A. Rathelot, P. L. Strick, Subdivisions of primary motor cortex based on cortico-motoneuronal cells. *Proc. Natl. Acad. Sci. U.S.A.* **106**, 918–923 (2009).
50. P. D. Cheney, E. E. Fetz, S. S. Palmer, Patterns of facilitation and suppression of antagonist forelimb muscles from motor cortex sites in the awake monkey. *J. Neurophysiol.* **53**, 805–820 (1985).
51. Y. Nishimura, S. I. Perlmutter, R. W. Eaton, E. E. Fetz, Spike-timing-dependent plasticity in primate corticospinal connections induced during free behavior. *Neuron* **80**, 1301–1309 (2013).
52. R. N. Lemon, G. W. Mantel, R. B. Muir, Corticospinal facilitation of hand muscles during voluntary movement in the conscious monkey. *J. Physiol.* **381**, 497–527 (1986).
53. P. Hník, R. Vejsada, S. Kasicki, Reflex and locomotor changes following unilateral deafferentation of rat hind limb assessed by chronic electromyography. *Neuroscience* **6**, 195–203 (1981).
54. S. H. Scott, T. Cluff, C. R. Lowrey, T. Takei, Feedback control during voluntary motor actions. *Curr. Opin. Neurobiol.* **33**, 85–94 (2015).
55. T. Takei, S. G. Lomber, D. J. Cook, S. H. Scott, Transient deactivation of dorsal premotor cortex or parietal area 5 impairs feedback control of the limb in macaques. *Curr. Biol.* **31**, 1476–1487.e5 (2021).
56. B. B. Edin, A. B. Vallbo, Dynamic response of human muscle spindle afferents to stretch. *J. Neurophysiol.* **63**, 1297–1306 (1990).
57. D. Flament, P. A. Fortier, E. E. Fetz, Response patterns and postspike effects of peripheral afferents in dorsal root ganglia of behaving monkeys. *J. Neurophysiol.* **67**, 875–889 (1992).
58. T. Umeda, T. Isa, Y. Nishimura, The primary motor cortex prospectively computes the spinal reflex. (bioRxiv, 2020); https://doi.org/10.1101/2020.06.29.170928.
59. T. Umeda, O. Yokoyama, M. Suzuki, M. Kaneshige, T. Isa, Y. Nishimura, Future spinal reflex is embedded in primary motor cortex output. (bioRxiv, 2023); https://doi.org/10.1101/2023.06.19.545500.
60. E. Taub, R. D. Heitmann, G. Barro, Alertness, level of activity, and purposive movement following somatosensory deafferentation in monkeys. *Ann. N. Y. Acad. Sci.* **290**, 348–365 (1977).
61. C. Darian-Smith, M. M. Ciferri, Loss and recovery of voluntary hand movements in the macaque following a cervical dorsal rhizotomy. *J. Comp. Neurol.* **491**, 27–45 (2005).
62. M. M. Morrow, L. E. Miller, Prediction of muscle activity by populations of sequentially recorded primary motor cortex neurons. *J. Neurophysiol.* **89**, 2279–2288 (2003).
63. D. Shin, H. Watanabe, H. Kambara, A. Nambu, T. Isa, Y. Nishimura, Y. Koike, Prediction of muscle activities from electrocorticograms in primary motor cortex of primates. *PLOS ONE* **7**, e47992 (2012).
64. M. Sato, On-line model selection based on the variational Bayes. *Neural Comput.* **13**, 1649–1681 (2001).
65. J. R. Dufresne, J. F. Soechting, C. A. Terzuolo, Electromyographic response to pseudo-random torque disturbances of human forearm position. *Neuroscience* **3**, 1213–1226 (1978).
66. J. Weiler, P. L. Gribble, J. A. Pruszynski, Spinal stretch reflexes support efficient hand control. *Nat. Neurosci.* **22**, 529–533 (2019).
67. M. H. Schieber, G. Rivlis, Partial reconstruction of muscle activity from a pruned network of diverse motor cortex neurons. *J. Neurophysiol.* **97**, 70–82 (2007).

Acknowledgments: We thank Y. Yamanishi for animal care, Y. Nishihara and M. Togawa for technical help, K. Seki for encouragement, and A. Pruszynski and S. Perlmutter for helpful discussions and critical comments. The monkeys used in this study were provided by the National Bioresource Project of the Ministry of Education, Culture, Sports, Science, and Technology of Japan (MEXT). **Funding:** This work was supported by grants from the Medtronic Japan External Research Institute, the Takeda Science Foundation and the Japan Agency for Medical Research and Development to T.U., a Grant-in-Aid for Scientific Research (19H01011 and 19H05723) to T.I., and the Strategic Research Program for Brain Sciences from MEXT, the Japan Agency for Medical Research and Development, the Japan Science and Technology Agency, Moonshot R&D, MILLENNIA Program (JPMJMS2012), and a Grant-in-Aid for Scientific Research from MEXT (23680061 and 25135733) to Y.N. **Author contributions:** Conceptualization: T.U., O.Y., T.I., and Y.N. Investigation: T.U., O.Y., M.S., M.K., and Y.N. Data curation: T.U., O.Y., and Y.N. Formal analysis: T.U. and O.Y. Methodology: T.U., O.Y., T.I., and Y.N. Resources: T.U., T.I., and Y.N. Software: T.U. Project administration: T.U., T.I., and Y.N. Supervision: T.I. and Y.N. Validation: T.U., T.I., and Y.N. Visualization: T.U., T.I., and Y.N. Writing–original draft preparation: T.U., O.Y., T.I., and Y.N. Writing–review and editing: T.U., O.Y., M.S., M.K., T.I., and Y.N. Funding acquisition: T.U., T.I., and Y.N. **Competing interests:** The authors declare that they have no competing interests. **Data and materials availability:** All data needed to evaluate the conclusions in the paper are present in the paper and/or in the Supplementary Materials. Source data are provided in this paper and can be found in the source data file. The MATLAB code and an example data are available on Zenodo repository at https://zenodo.org/records/10623537.

Submitted 22 May 2024
Accepted 13 November 2024
Published 18 December 2024
10.1126/sciadv.adq4194